ADVANCED FUNCTIONAL MATERIALS

Supporting Information

for *Adv. Funct. Mater.,* DOI: 10.1002/adfm.201707134

Scalable and Highly Efficient Mesoporous Wood-Based Solar Steam Generation Device: Localized Heat, Rapid Water Transport

*Tian Li, He Liu, Xinpeng Zhao, Guang Chen, Jiaqi Dai, Glenn Pastel, Chao Jia, Chaoji Chen, Emily Hitz, Das Siddhartha, Ronggui Yang, and Liangbing Hu**

Supplementary Information

The thermal confinement properties of our vertically-cut mesoporous benefit the solar steam generation efficiency greatly. As shown in the schematics of Figure S1(a-c), the impediment of thermal conduction through wood in the cross-lumen direction helps confine thermal energy to the top surface of the vertically-cut wood. The thermal energy can thus be concentrated within the thin graphite layer. In contrast, the thermal energy of horizontally-cut wood cannot be concentrated due to the penetrating graphite powder into the lumens and the higher thermal conductivity along the lumen direction (Figure S1(d-f)). As illustrated in Figure S1(b) and (e), the heat generated by radiative energy sources is preferably directed in the wood lumen direction (exhibiting an elliptical thermal pattern from top view) in vertically-cut wood. We also experimentally showed that the thermal insulation of anisotropic vertically-cut wood is even better than that of Styrofoam (isotropic, 0.03 W/m·K) owning to the re-directed heat transfer along the in-plane direction. Thus, the conductive heat loss across the lumen direction through water can be largely reduced. The resulting elevated surface temperatures and evaporation rates under varied solar intensities are compared for vertically-cut and horizontally-cut wood in Figure S1(g). Notably, for the first time, we showed that the fluidic transport across the lumen direction can supply a sufficient flow of water for steam generation. Detailed experimental results can be found in Figure 2d and 2e where a fast fluidic transport rate of 0.5 mm/s was demonstrated. Simulation results help elucidate the mechanisms responsible for fast fluidic rates across the lumen direction (Figure 2f). Combining the innovative utilization of fluidic transport of pits in the radial direction and realization of thermal confinement due to the anisotropic thermal conductivity in wood, our device with vertically-cut wood exhibits a record-high one Sun efficiency among all bio-material based solar steam devices[27,28,33], much higher than devices based on horizontally-cut wood (Figure S1(i)). The record-high one-Sun efficiency and scalability of these devices renders our demonstrated approach extremely promising for practical applications.

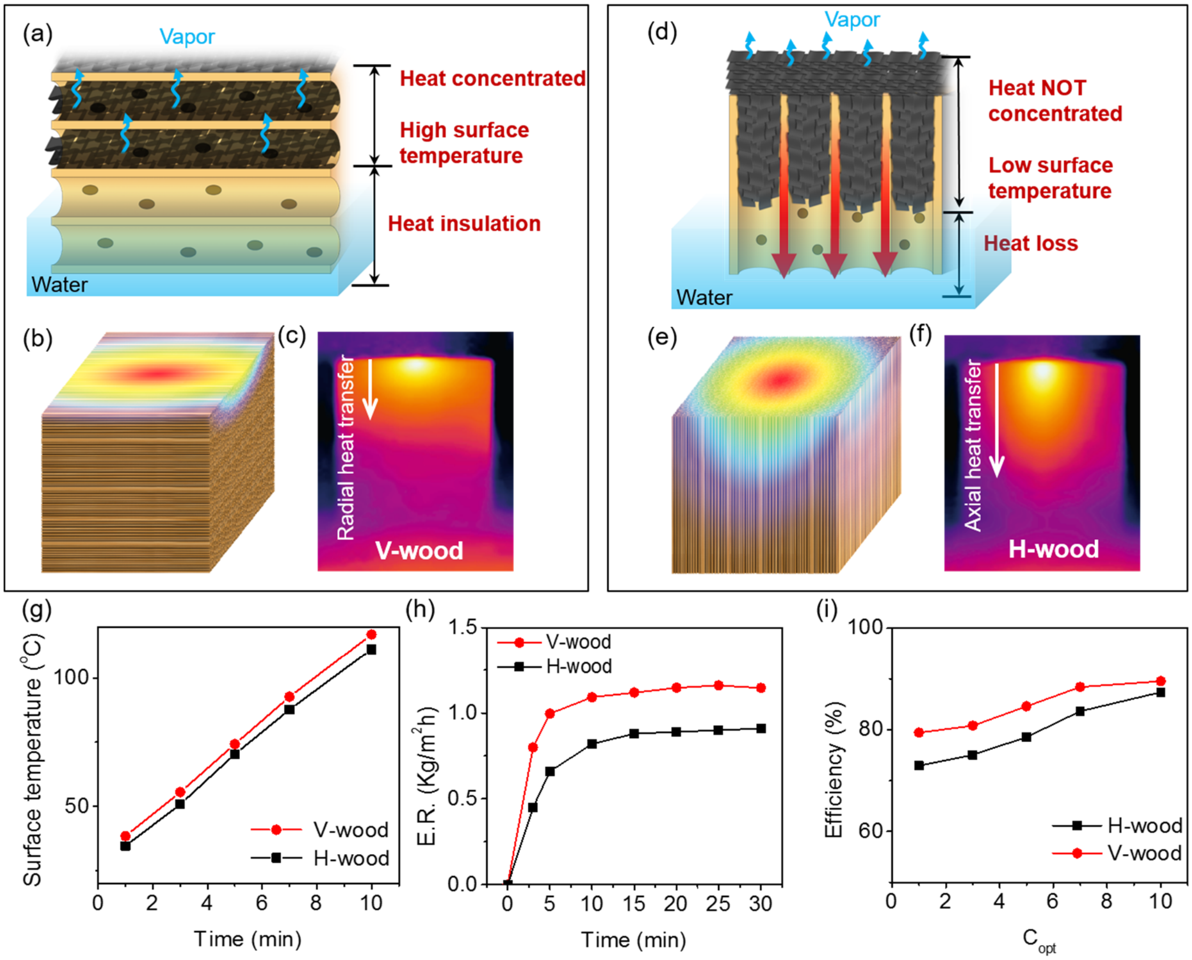

Figure S1. **Comparison between vertically cut wood and horizontally cut wood in solar steam generation.** (a) Schematic of the solar steam generation process with vertically cut wood in which heat can be concentrated on the top surface without much conductive heat loss to the water and surroundings. (b) Schematic showing the heat confinement in vertically cut wood. (c) IR image showing the heat profile in vertically cut wood. (d) Schematic of the solar steam generation process with horizontally cut wood where heat cannot be concentrated on the top surface due to the penetrating graphite power in the wood lumens and the increased conductive heat loss to the water and surroundings. (e) Schematic showing the heat loss in horizontally-cut wood. (f) IR image showing the heat profile in horizontally cut wood. (g) Comparison of the surface temperature between vertical and horizontally cut wood. (h) Comparison of the evaporating rate between vertically and horizontally cut wood. (i) Comparison of the solar steam generation efficiency between vertically and horizontally cut wood.

Supplementary Discussion | Analysis of anisotropic thermal conductivity of wood

Wood has been used for thermal insulation material for decades. However, studies and applications utilizing the anisotropic thermal conductivity of wood are rare. Generally speaking, owing to the natural alignment of wood lumens and the large porosity of wood, heat conduction in the axial direction is much larger than in the transverse direction. We innovatively utilized the anisotropic thermal conductivity of wood to help with heat confinement in the solar energy receiving layer while impeding the conductive heat transfer into the wood matrix (water supply channels).

A simple model can be used to estimate the effective thermal conductivity in both the axial and radial directions. Due to its low application temperature and low emissivity, radiative heat transfer is neglected in the following analysis.

$$\lambda_{e\perp} = \frac{\lambda_{f\perp}\lambda_g}{(1-\varphi)\lambda_g + \varphi\lambda_{f\perp}} \quad (3)$$

$$\lambda_{e//} = (1-\varphi)\lambda_{f//} + \varphi\lambda_g \quad (4)$$

where, $\varphi \approx 0.70$, is the porosity of wood, $\lambda_{f//}$ and $\lambda_{f\perp}$ is thermal conductivity of microfibril along the chain and perpendicular the chain, and $\lambda_g = 0.026$ W/m·K is the thermal conductivity of open pores (filled with air). The predicted thermal conductivities of natural wood in the axial and transverse directions are $\lambda_{e\perp} = 0.07$ W/m·K and $\lambda_{e//} = 0.33$ W/m·K, respectively, which agrees with the measurement results ($\lambda_{e\perp} = 0.106$ W/m·K and $\lambda_{e//} = 0.35$ W/m·K) very well.

In our design, the use of the vertical direction of wood (V-wood) can greatly reduce the heat loss from the graphite layer to the water, much better than H-wood (Figure R5). Thus, the larger energy concentration and higher surface temperature can be acquired in graphite layer, which further improve the solar steam efficiency.

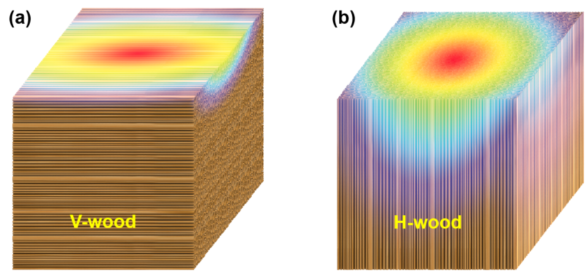

Figure S2. Schematic of anisotropic thermal properties of wood. (a) Thermal energy tends to spread along wood lumen direction with impeded heat transfer into wood matrix in vertically cut wood (b) Thermal energy tends to penetrate into wood matrix in horizontally cut wood.

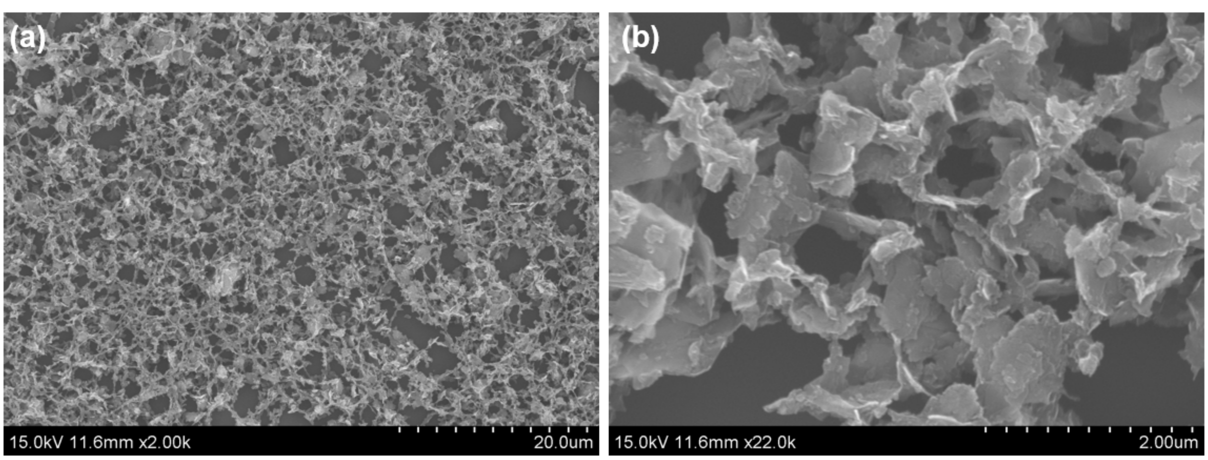

Figure S3. SEM images of sprayed-on graphite flakes (a) A uniform layer of graphite flakes was deposited by spraying. A network of graphite flakes was formed uniformly by spraying. (b) The graphite flakes exhibit an average size of ~0.5 μm.

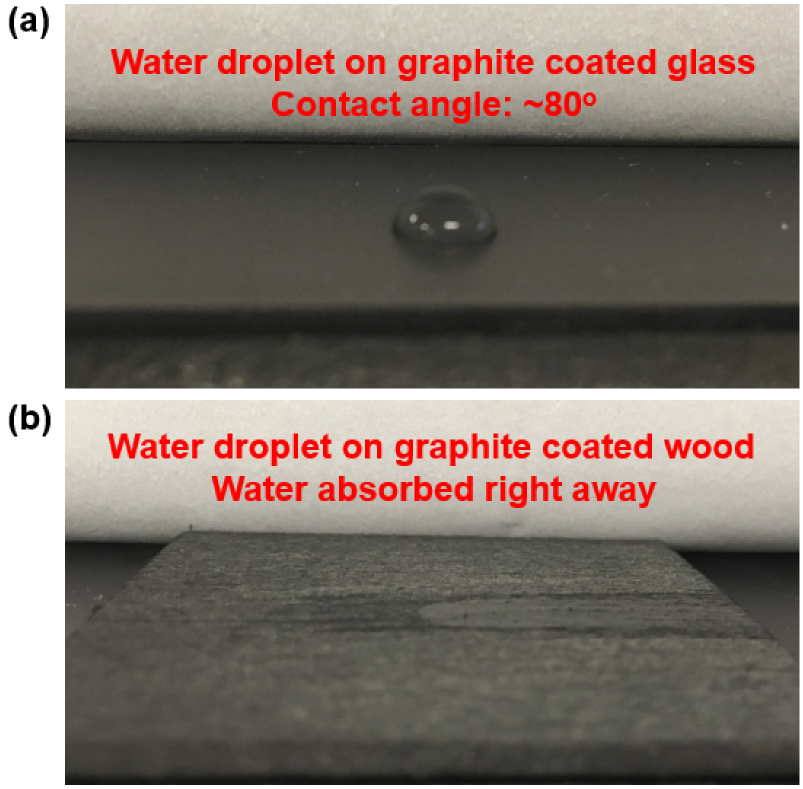

Figure S4. Wettability of sprayed-on graphite on vertically cut wood. (a) A layer of graphite was sprayed on glass. The water droplet on the graphite layer exhibits a contact angle of ~ 80^{o}. (b) A layer of graphite was sprayed on wood. The water droplet was absorbed right away.

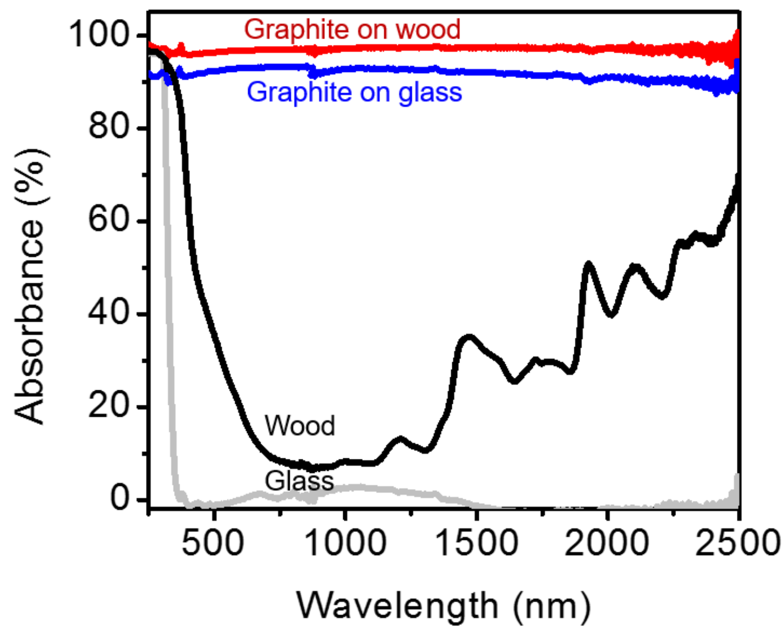

Figure S5. UV vis absorption spectrum of glass, wood, graphite flakes sprayed on glass and graphite flakes sprayed on wood.

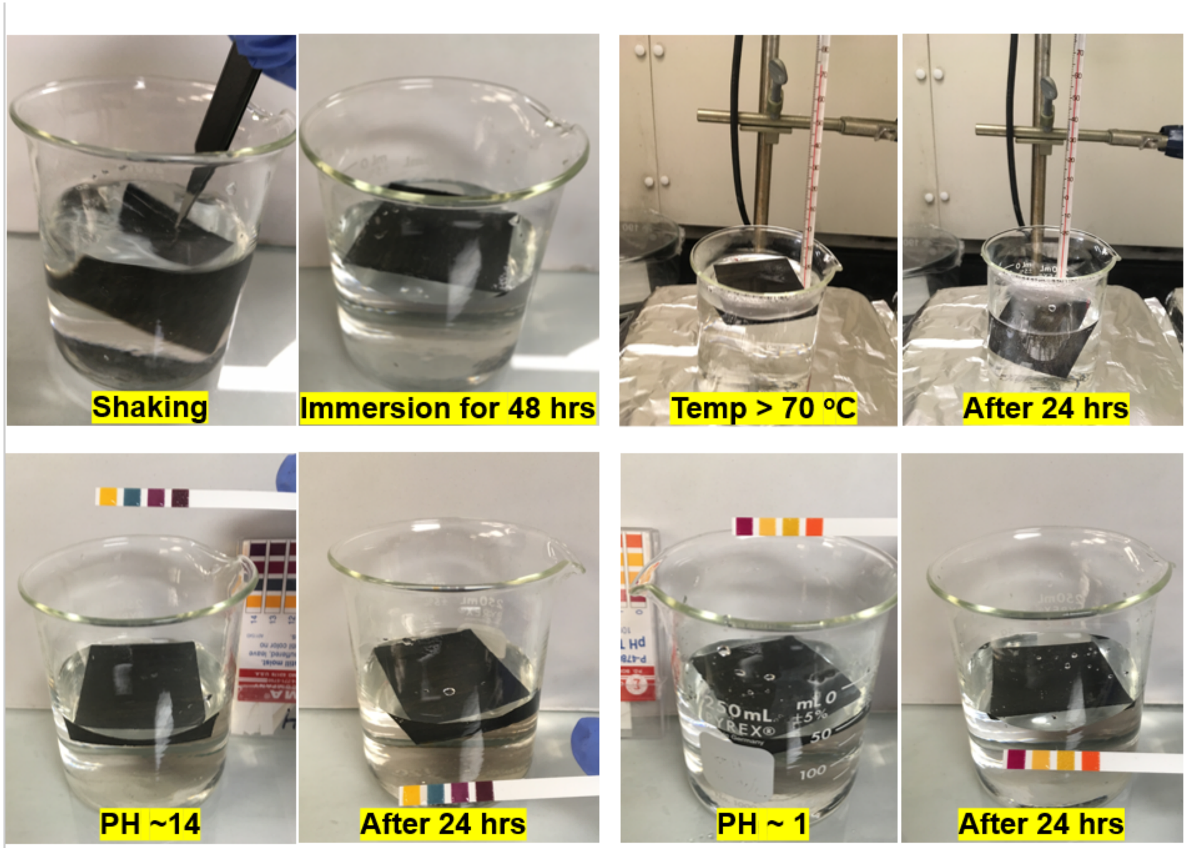

Figure S6. Stability test of graphite wood under various conditions: (a) shaking and immersing in water for 48 hours (b) ~70^{o}C for 24 hrs (c) alkaline environment of PH ~14 for 24 hrs (d) acid environment of PH ~1 for 24 hrs. The results show no notable detachment of graphite under harsh conditions.

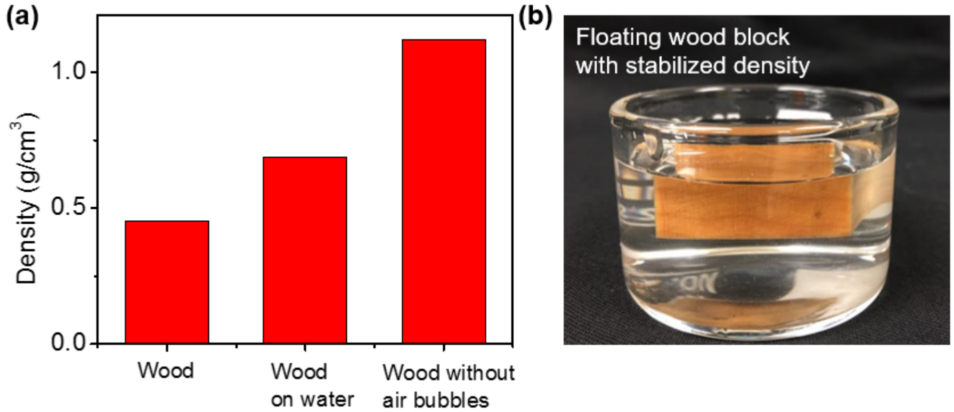

Figure S7. (a) Density of basswood, stabilized density of basswood after floating on water for 48 hrs, density of basswood with fully infiltrated water inside of wood lumens achieved after vacuum infiltration. (b) Photo image of a floating wood block after 48 hrs.

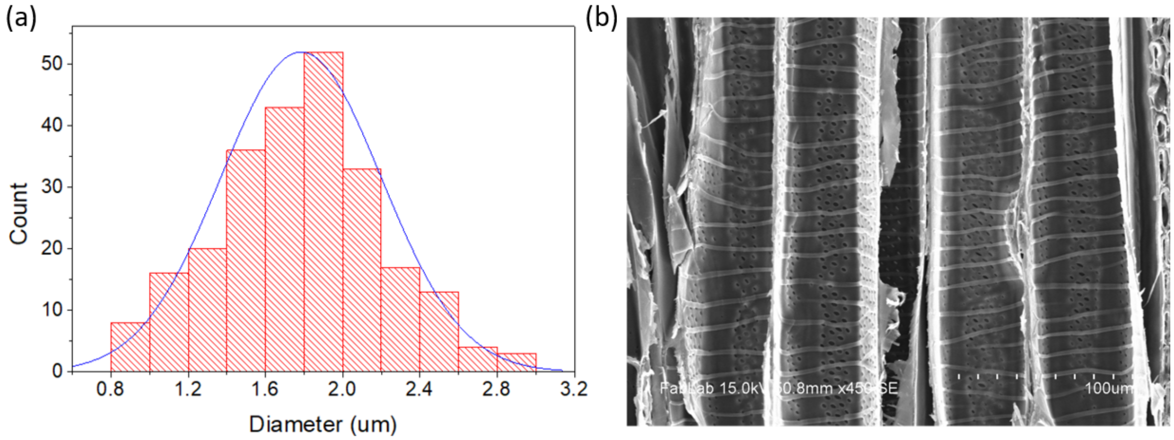

Figure S8. (a) Size distribution of the pits on wood lumens. (b) SEM image of the pits on wood lumens.

The absorbance when the light is at an angle of 90^o and 45^o was compared. As can be seen, the absorbance exhibits minimum variation. This is potentially due to the mesoporous top surface of wood which effectively traps incoming light.

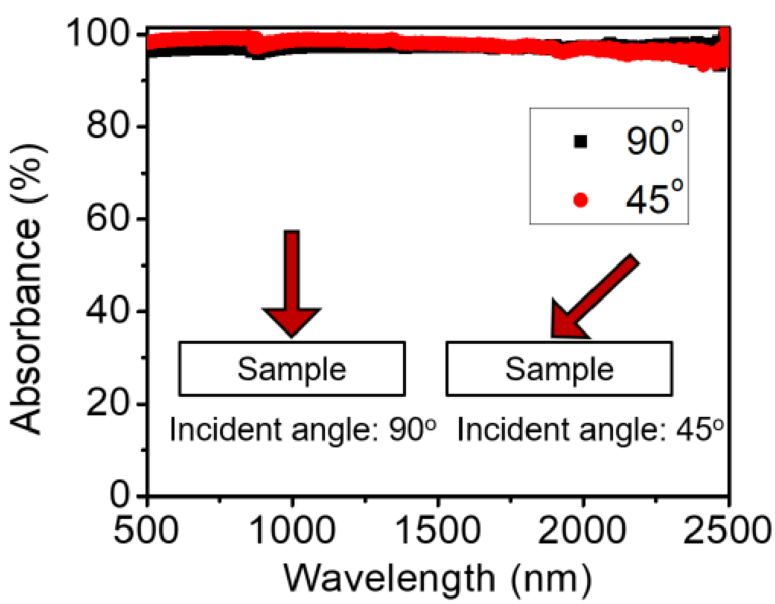

Figure S9. Absorbance of graphite coated wood with different incident angles.